ceramics

MDPI

Review

3D Printing Ceramics—Materials for Direct Extrusion Process

Eliza Romanczuk-Ruszuk [1,*], Bogna Sztorch [2], Daria Pakuła [3], Ewa Gabriel [2,3], Krzysztof Nowak [3] and Robert E. Przekop [2,*]

[1] Institute of Biomedical Engineering, Faculty of Mechanical Engineering, Bialystok University of Technology, Wiejska 45C Street, 15-351 Bialystok, Poland
[2] Centre for Advanced Technologies, Adam Mickiewicz University in Poznań, Uniwersytetu Poznańskiego 10 Street, 61-614 Poznań, Poland
[3] Faculty of Chemistry, Adam Mickiewicz University in Poznan, Uniwersytetu Poznańskiego 8 Street, 61-614 Poznań, Poland
* Correspondence: e.romanczuk@pb.edu.pl (E.R.-R.); rprzekop@amu.edu.pl or r.przekop@gmail.com (R.E.P.)

Abstract: Additive manufacturing and 3D printing methods based on the extrusion of material have become very popular in recent years. There are many methods of printing ceramics, but the direct extrusion method gives the largest range of sizes of printed objects and enables scaling of processes also in large-scale applications. Additionally, the application of this method to ceramic materials is of particular importance due to its low cost, ease of use, and high material utilization. The paper presents the most important literature reports on ceramics printed by direct extrusion. The review includes articles written in English and published between 2017 and 2022. The aim of this literature review was to present the main groups of ceramic materials produced by extrusion-based 3D printing.

Keywords: 3D printing; ceramics; fused deposition of ceramics; additive manufacturing; paste extrusion

Citation: Romanczuk-Ruszuk, E.; Sztorch, B.; Pakuła, D.; Gabriel, E.; Nowak, K.; Przekop, R.E. 3D Printing Ceramics—Materials for Direct Extrusion Process. *Ceramics* **2023**, *6*, 364–385. https://doi.org/10.3390/ceramics6010022

Academic Editor: Manuel Belmonte

Received: 21 November 2022
Revised: 15 January 2023
Accepted: 28 January 2023
Published: 1 February 2023

1. Introduction

Ceramics are considered high-performance materials due to their hardness, high resistance to wear, temperature, corrosion, and good mechanical properties. Ceramics with special properties are used in modern industries such as energy, aviation, military and chemical industries, additionally in mechatronics and biomedical applications [1]. The manufacture of ceramic products by the traditional method is divided into three stages: material preparation, forming (the most labor-intensive), and sintering. The forming of ceramic materials is carried out in various ways, such as isostatic pressing, injection molding, or slip casting. The technological process of each of these methods is different, but most of them use molds. Therefore, the disadvantage of these methods is the limitations that arise from the use of special equipment [1–3]. Another disadvantage is the limited complexity of the manufactured component, due to the simple geometric shapes of the molds. The materials are further machined, which are difficult to manufacture due to the brittleness of ceramics [1,4].

Materials that are used in additive manufacturing and 3D printing can be divided according to the adaptation to the selected production process (e.g., powders, fibers, and pastes) or according to the type of material (e.g., metals, polymers, and ceramics) [5,6]. The material in the production process is selected according to the use of a specific element. At the same time, it should have good physical properties and appropriate mechanical strength after the process, which can be improved with further processing [7]. Recently, there has been a lot of work on new polymer and metallic materials for 3D printing [8–11]. It is worth noting that there are many studies on the 3D printing of ceramics [4,12–14]. Ceramic materials are used in various AM techniques, such as material extrusion, binder jetting, and directed energy deposition [15]. However, extrusion-based processes are the most popular because of the low cost of the equipment used in this technique. In addition, it is possible to use different materials and the material losses in the manufacturing process

are low [16]. The main extrusion-based ceramic manufacturing processes include Fused Deposition of Ceramics, Extrusion Freeform Fabrication, Robocasting, Thermoplastic 3D Printing, and Freeze-Form Extrusion Fabrication [15].

Generally, in the literature, we can find various groups of ceramic materials that are produced by 3D printing from fused ceramic deposition. The authors of this paper divided ceramic pastes into the following groups: oxides, non-oxides, mixed oxides, bioceramics, clays, and cementitious materials (Figure 1).

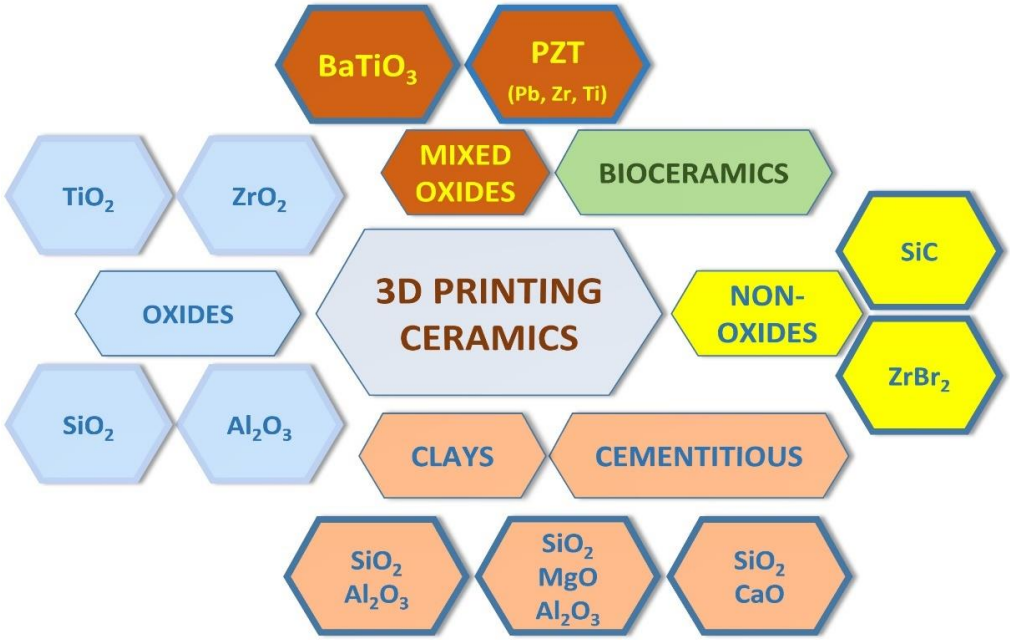

Figure 1. Schematic of the classification of ceramic materials.

In the last decades of the 20th century, the technology of additive manufacturing (AM) and 3D printing has developed significantly. It is one of the fastest-developing technologies in recent years, and therefore it is considered to be part of the new industrial revolution [17–19]. In additive manufacturing, three-dimensional models are used to form the component layer by layer. Therefore, it is possible to manufacture components with non-standard dimensions and architectures and with different chemical compositions on a micro/molecular scale [1]. The advantage of 3D printing, which affects the fast development of this technology, is the possibility of creating products with a complicated shape and reducing processing procedures, such as making additional molds, using multiple machine tools. Notably, 3D printing provides design and production integration and can realize high-efficiency and high-speed manufacturing. Moreover, the more complicated the shape of the produced element is, the more reasonable it is to use 3D printing [8,20]. Therefore, 3D printing is becoming an increasingly popular method of manufacturing components used in various fields such as automotive, electronics, aerospace, chemical industry, and biomedical engineering (Figure 2) [1,9,21]. In 2020, the total AM market was valued at approx. EUR 7 billion, additionally, the compound annual growth rate was estimated at approx. 20% by 2025 [22].

The ISO/ASTM 52,900 standard describes the issues related to additive manufacture, in which seven categories of AM are presented [23]: (a) binder jetting, (b) direct energy deposition, (c) material extrusion, (d) material jetting, (e) powder bed fusion, (f) sheet lamination, and (g) vat photopolymerization.

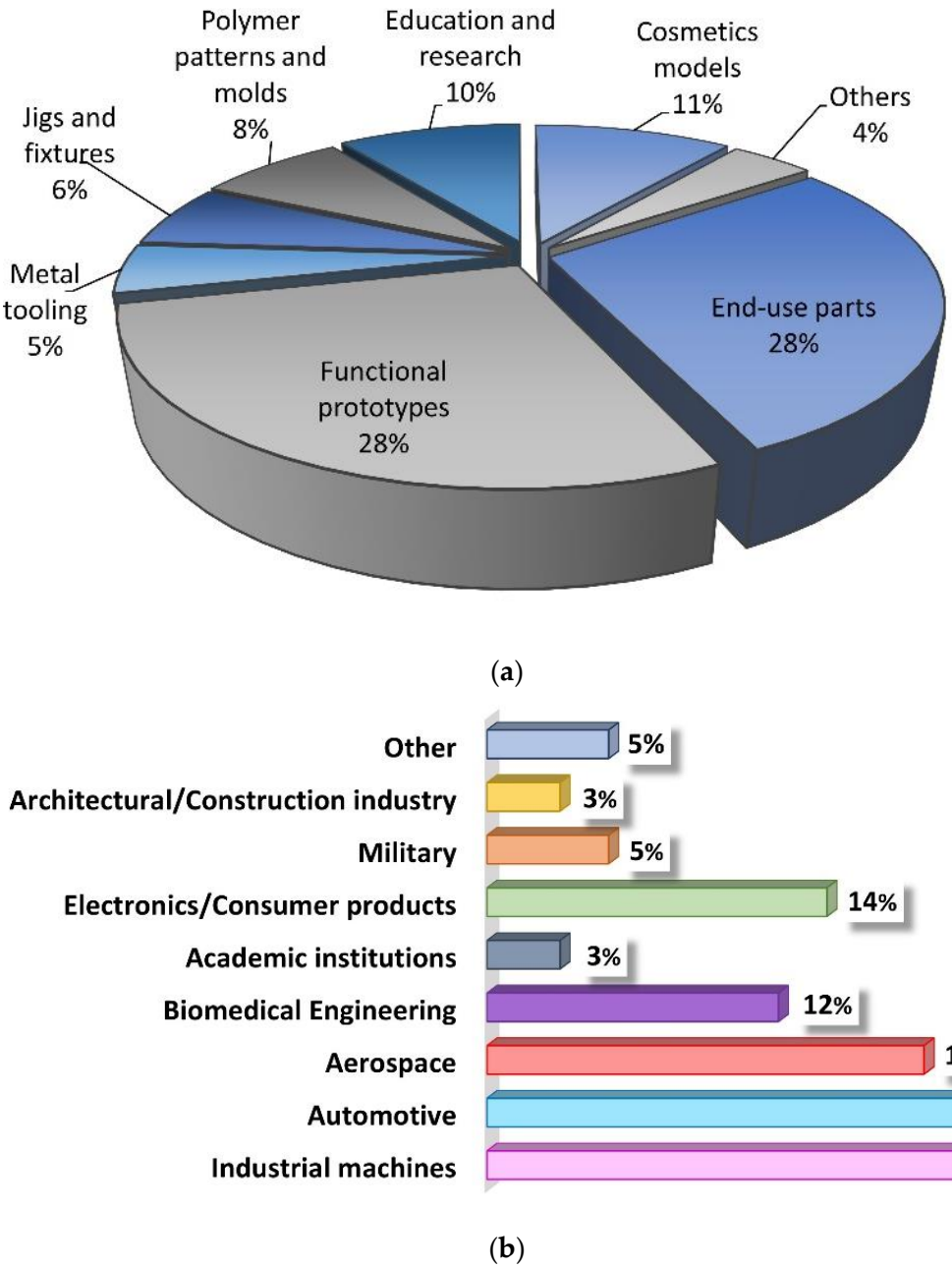

Figure 2. (**a**) AM application in production; (**b**) the use of AM in various industrial sectors [1,9,21].

Based on the Scopus analysis, a growing trend in the number of publications for the keywords '3D printing' and 'ceramics' can be seen (Figure 3). The analysis shows that from 1993 to 2023, there are 2594 scientific articles. In the last three years, i.e., 2020, 2021, and 2022, the number of publications is 1379, which is over 53% of all publications from 1993 to 2023. By 2014, 227 articles had been published. After 2014, there is a significant increase in the number of works on 3D printing and ceramics, which indicates a breakthrough moment for this field. In the period 2015–2023, 2367 papers were published. This is related to the development of additive techniques, and thus the search for new methods of printing, process optimization, or research on compositions for printing, which will ensure, for example, the improvement of some physicochemical properties while reducing production costs.

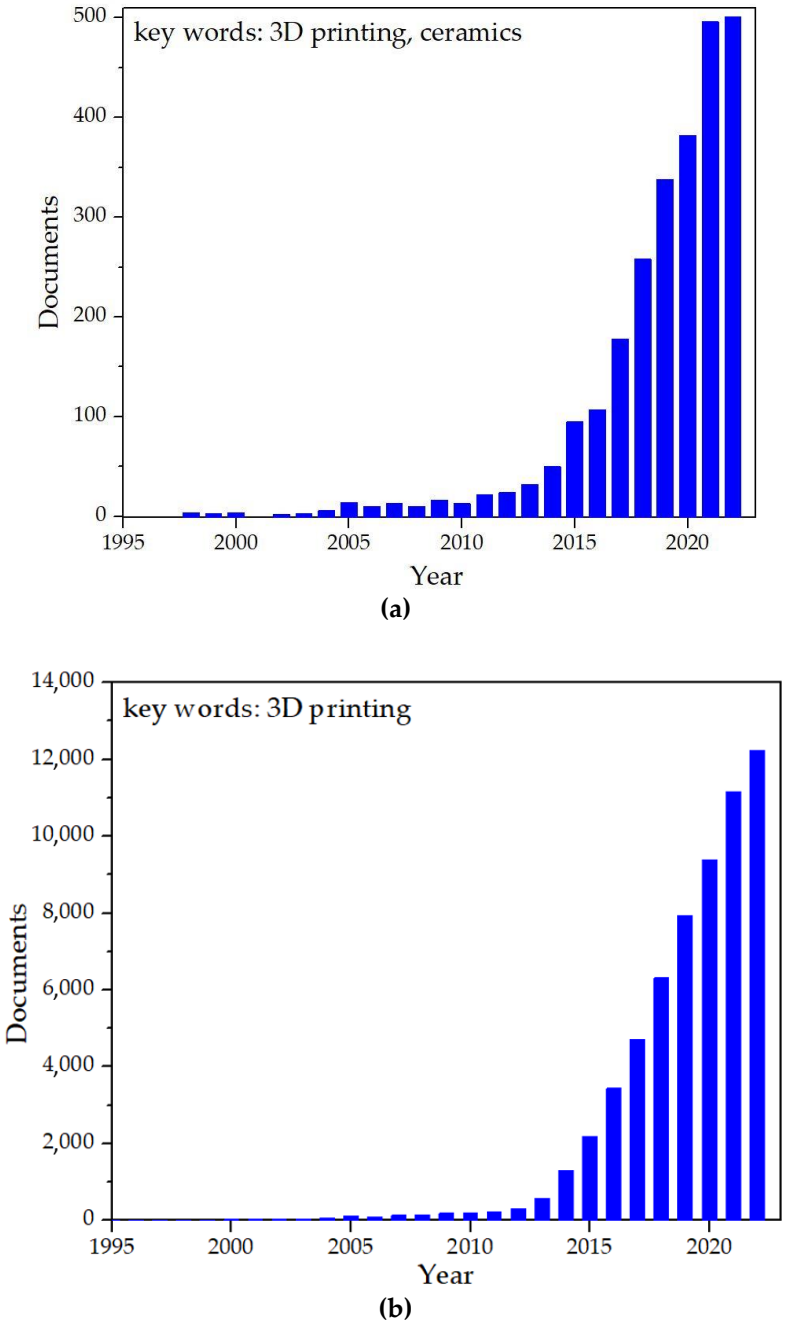

Figure 3. Scopus keywords: (**a**) 3D printing and ceramics and (**b**) 3D printing.

This review will focus on the 3D printing of ceramics using the extrusion method, especially the fused deposition of ceramics and paste deposition modeling. Because there are many publications describing and comparing the techniques of additive manufacturing of ceramic materials via the extrusion method, the authors will focus on presenting ceramic materials that are used in this method, especially for ceramic pastes.

2. Fused Deposition of Ceramics

The literature review shows that there is no specific terminology regarding the 3D printing of ceramics. The authors [5,8,15,24] differently define the process of direct deposition of ceramic materials, such as Fused Deposition of Ceramics (FDC), Paste Deposition Modeling (PDM), Extrusion Freeform Fabrication (EFF), Direct Ink Writing (DIW).

Fused deposition of ceramics is often described as printing a thermoplastic filament with embedded ceramic particles (at a maximum volume of 60%). The filament is partially melted and extruded from a moving head layer by layer. Another approach is to use a ceramic slurry that is extruded from a die to form a fiber [24,25]. Therefore, in this work, the authors will focus on the 3D printing of ceramic pastes and will use the term fused deposition of ceramics (FDC).

Fused deposition of ceramics is a process based on the extrusion of ceramic paste in the form of a filament [7]. The process can be described in the following steps. In the first step, the ceramics are mixed with dispersants, solvents, and other phases until a homogeneous ceramic paste is obtained. Then, the paste is filled into a cartridge and extruded through a die, while the cartridge moves in computer-controlled x- and y-directions and forms into a 3D shape. Ceramic paste should have a high concentration of ceramic powder and a thixotropic flow. The final step is high-temperature sintering of the 3D-printed ceramic element [8,26]. Figure 4 shows a schematic of a fused deposition of ceramics.

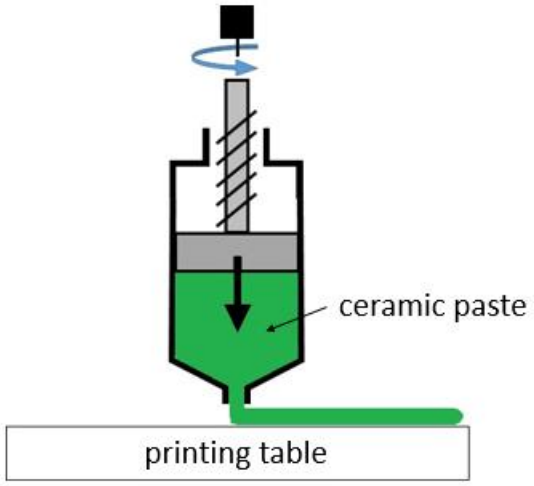

Figure 4. Schematic of a fused deposition of ceramics (FDC) [27].

Ceramic paste 3D printers can be divided into two groups, which differ in the way of feeding the material, namely, the separation of the container from the moving parts. There are devices that perform extrusion in a one-step process and devices in which the first step is material feeding and the second step is extrusion (two steps) (Figure 5).

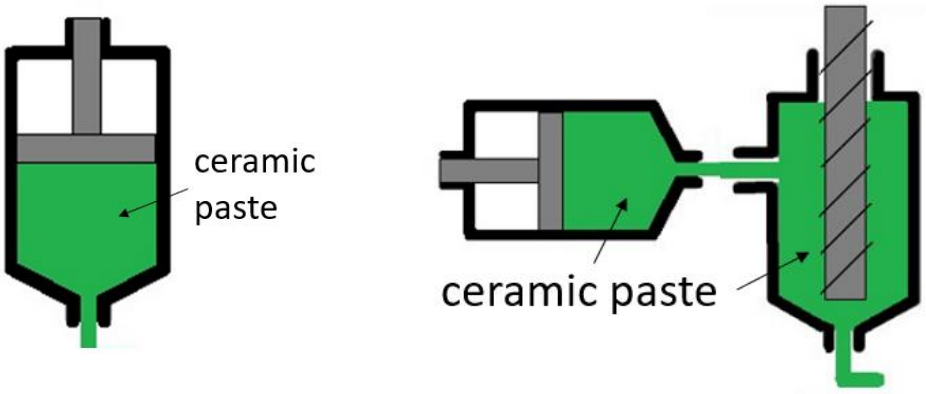

(**a**) (**b**)

Figure 5. Schematic of one-step (**a**) and two-step (**b**) printing devices [17,27].

The two-step process is often used in 3D printing to print large parts, usually from cement or cement-based materials. A typical concrete 3D printing process consists of four main stages: mixing, pumping, extruding, and building. A concrete 3D printer consists of a manipulator in the form of a robotic arm or a crane system that moves the print head to apply concrete along a defined path (Figure 6) [28].

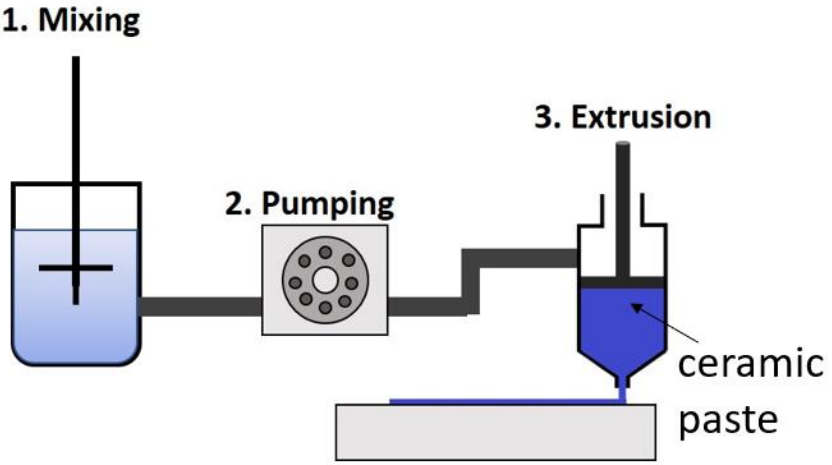

Figure 6. Schematic of a concrete 3D printer [28].

In 3D printing with material extrusion, two main elements can be distinguished: a printer, which is responsible for the movement of the nozzle, and an extruder through which the material is fed and which controls the material flow. Extruders may differ in the extrusion system: (a) the piston is driven by a stepper motor, (b) a pneumatic piston, and (c) a screw conveyor (Figure 7) [29,30].

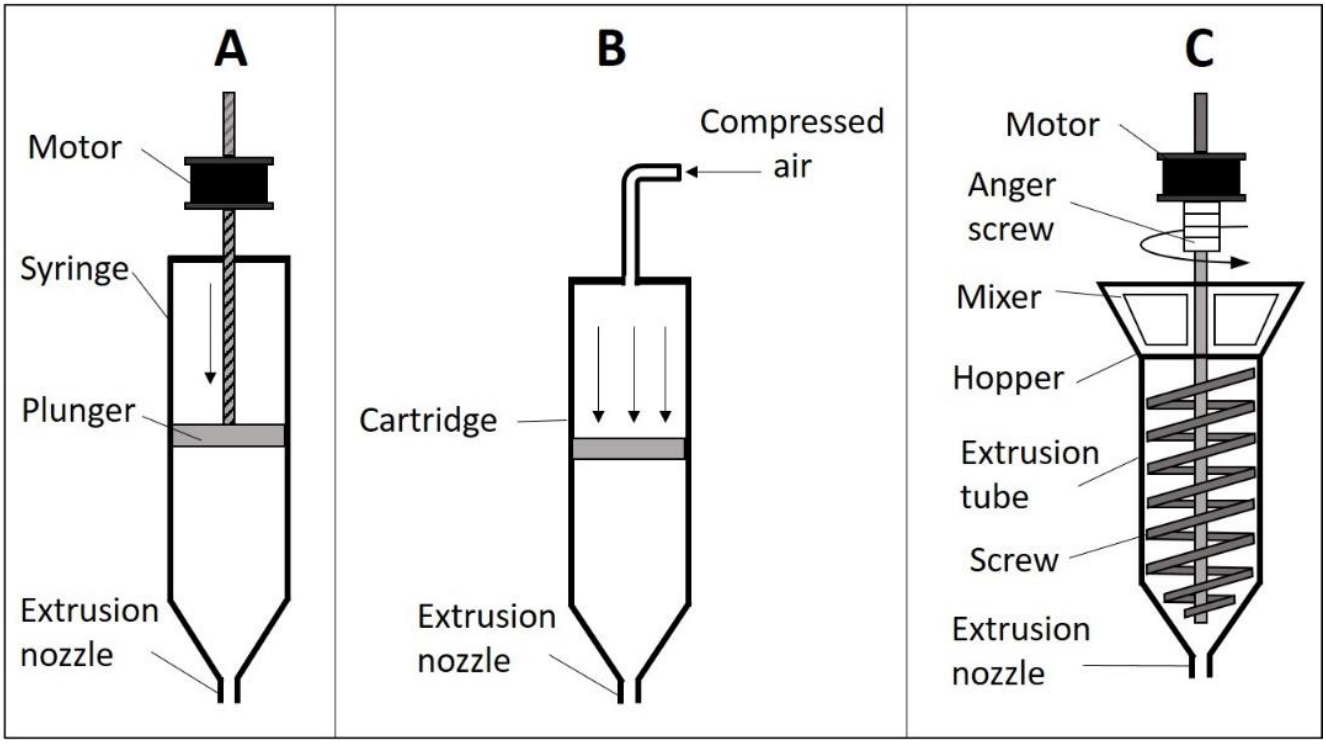

Figure 7. Schematic of extrusion systems: (**A**) syringe-based extrusion, (**B**) air pressure-driven extrusion, and (**C**) screw-based extrusion [30].

In an extruder using a piston-driven stepper motor, the material is in physical contact with the piston. In this method, it is possible to control the extrusion rate more accurately compared to other systems, because the system provides a constant displacement of the volume. In addition, there is a delay in the start and end of the extrusion process here, and as a result, the print may be inaccurate [31].

The driving force of extrusion in a pneumatic extrusion system is compressed gas. The most commonly used gas is air, but it can be replaced by nitrogen if sterility is required, especially in printing with biological inks. Pneumatic extrusion allows the printing of viscoelastic materials. In addition, this method provides a faster response time to print errors because the cartridge can be depressurized rapidly. This system requires the use of compressed gas and is therefore more complex to build compared to systems with a stepper motor [32,33].

In a system with a screw conveyor, a single screw extruder is used to supply material from the hopper to the nozzle. The rotary screw mixes the material during printing and ensures uniformity of structure and prevents phase separation. There are limitations to the materials used in this method. Soft materials such as cells are not printed with a screw extruder, as the shear force could damage the cell membrane [33,34].

3. Ceramic Pastes Used in the FDC Method

3.1. General Properties of Ceramic Pastes

Ceramic pastes used in the FDC method are characterized by high plasticity; therefore, they can be extruded. These materials can be homogeneous and heterogeneous, containing solids, water, and additives, which can be polymer plasticizers or inorganic electrolytes. The rheological properties of pastes are important due to the technological process and the final quality of the product, and it can be regulated by the grain size of solid particles (optimization of the grinding process) and the selection of past components with lower/higher plasticity [27,35].

As mentioned earlier, additives such as plasticizers, binders, and suitable dispersants are added to the preparation of printing pastes. Their function is to regulate particle dispersion and viscosity, as particle volume affects viscoelastic properties: storage modulus (G′) and loss modulus (G) [36,37]. The flow through the nozzles is allowed by the shear-thinning properties as the viscosity of the paste is reduced by several orders of magnitude and thus the shear rate is increased when an external force is applied to the extruded material. Moreover, after printing, the properties of the paste change due to evaporation and drying of the solvent, and the ceramic paste changes from pseudoplastic to dilatation. Ceramic pastes with high solids content and defined rheological properties, after extrusion from small diameter nozzles, retain their physical integrity and maintain their weight without deformation, and therefore it is possible to print elements layer by layer [36,38,39].

In general, the rheological properties are determined on the basis of the relationship between the external force and their reaction as flow or deformation. Rheological properties are important for the FDC method, and on their basis, appropriate technical parameters of 3D printing are selected, such as extrusion pressure [27,40].

3.2. Classification of Ceramic Pastes

As mentioned in the introduction, in this work, ceramics printed with the FDC method were divided into the following groups: oxides, non-oxides, mixed oxides, bioceramics, clays, and cementitious materials (Table 1). The authors presented and discussed the works from 2017 to 2022.

Table 1. Groups of materials used in FDC printing.

Group of Materials	Material Used	Binder/ Additions	Application	Refs.
Oxides	Aluminum oxide (Al_2O_3)	glycerin, boehmite nanoparticles (AlO(OH)), aluminum dihydrogen phosphate ($Al(H_2PO_4)_3$, AP), CuO and TiO_2;	catalysts	[41–43]
	Titanium oxide (TiO_2)	modified titanium diisopropoxide bisacetylacetonate (TIA), polyvinyl alcohol (PVA), zinc, TALH (Ti(IV) bis (ammonium lactato) dihydroxide);	biomedical engineering, filtration, energy industry	[44–47]
	Zirconium oxide (ZrO_2)	yttrium oxide stabilized zirconium powder (YZS), polyvinyl alcohol (PVA), polyethylene glycol (PEG-400), L-ascorbic acid (AA), citric acid (CA), Methocel, Darvan 821A, glycerol, Agitan 299 and polyethyleneimine;	biomedical engineering	[48–50]
Mixed oxides	Lead zirconate titanate (PZT)	polyvinyl alcohol (PVA), ammonium polyacrylate;	piezoelectric transducers, acoustic sensors, energy harvesting	[51,52]
	Barium titanate ($BaTiO_3$—BT)	polyvinylidene fluoride (PVDF), N,N-dimethylformamide (DMF), polyvinyl alcohol (PVA);	capacitors, multilayer capacitors, sensors, and energy storage devices	[53–56]
Non-oxides	Zirconium diboride (ZrB_2)	polyvinyl alcohol (PVA), sodium 1-heptanesulfonsodium 1-heptanesulfonate (C7), sunflower oil;	ultra-high-temperature applications, aerospace, nuclear reactor	[57–60]
	Silicon carbide (SiC)	liquid silicon, n-hexane mixed with polycarbosilane (PCS), distilled water, dispersing agent (Tamol NN 9401), glycerol, n-hexane (PCS solvent), and toluene;	aerospace and military industries, nuclear applications, sensors	[61–65]
Bioceramics	Hydroxyapatite (HA)	polyvinyl butyral (PVB), polyethylene glycol (PEG), propan-2-ol, hydroxy propyl methyl cellulose (HPMC);	bone tissue engineering (scaffolds)	[66–68]
	Calcium phosphate (CaP)	Dolapix CE 64 anionic surfactant, polyvinylpyrrolidone (PVP);	biomedical engineering	[67–70]
Clays	Kaoline ($2SiO_2 \cdot Al_2O_3 \cdot 2H_2O$)	sodium silicate, sodium polyacrylate;	pottery, catalysts	[71–74]
Cementitious materials	Ordinary Portland Cement	fly ash, blast furnace slag, silica fume, polyvinyl alcohol fiber (PVA), hollow glass microspheres (HGMs);	construction	[75–77]

3.2.1. Oxides

Aluminum Oxide

The ceramics processing industry over the last decade has been strongly focused on the production of structurally complex three-dimensional objects with specific functional and mechanical properties. The scientific community sees the special potential of the additive manufacturing technology of ceramic materials in the 3D printing of catalysts. The macroscopic structure of solid catalysts affects the efficiency of heat and mass exchange in chemical transformations, the dynamics of the flow of reactants, and the increase in catalytic efficiency. Alvarez et al. in the work entitled: "Optimization of the sintering thermal treatment and the ceramic ink used in direct ink writing of α-Al_2O_3: Characterization and catalytic application." Notably, [41] described research aimed at optimizing both the formulation of ceramic paste and the thermal treatment of 3D objects. In addition, novel catalysts with different geometries and packings were developed to enhance catalytic efficiency. In this work, the reaction of catalytic conversion (dehydrogenation) of ethanol was used for testing purposes. Aluminum oxide (Al_2O_3) and gelling material dissolved in distilled water were used to prepare the printing pastes. Al_2O_3 has several allotropes. In the described publication, the thermodynamically stable α form was used in the research. The results of experimental studies have been presented, which show that the optimal sintering conditions to obtain the best microstructural and mechanical properties are subjecting the sample to a temperature of 1550 °C (1823 K) for 6 h. It was also noticed that the dimensional stability of the prints increases with the increase in the concentration of the ceramic powder.

However, a higher content of Al_2O_3 causes an increase in shear stress and the need to apply a higher pressure during the material dispensing process. In this study, a ceramic paste was selected for which both mechanical and printability properties were at a sufficiently optimal level and is 70% Al_2O_3 [42]. The studies of the packing geometry showed that the catalytic efficiency is directly related to the size of the catalyst surface. The authors proved that the structures of FDC-printed catalysts, compared to those commercially available with similar volume, show longer residence time, resulting in better catalytic performance [41].

Due to properties such as chemical and thermal stability, relatively good mechanical strength, good electrical and thermal insulation, and high availability, alumina is a material often used for engineering applications. In the work of Finke et al. [42], modifications of Al_2O_3 pastes by adding substances changing rheological properties were described. Part of the liquid phase was replaced with glycerin, while boehmite nanoparticles (AlO(OH)) partially replaced Al_2O_3. This resulted in a series of pastes with equal total solids content. The results showed that the influence of AlO(OH) on shear thinning is significantly greater than that of the liquid additive. In addition, nanoparticles of boehmite increase mechanical strength [42].

A compatible inorganic binder for Al_2O_3-based materials is aluminum dihydrogen phosphate ($Al(H_2PO_4)_3$, AP), which strengthens Al_2O_3 ceramics by chemically bonding phosphate phases. In the work of Xin Xu et al., [43] describes the influence of AP agglomerates on dimensional shrinkage properties, mechanical strength, and printability.

In contrast to organic binders, which undergo a pyrolysis process during sintering, resulting in high shrinkage, inorganic binders, e.g., the aforementioned AP, contribute to greater dimensional stability, which is very important in printing with ceramic materials and is often a significant challenge. The aim of the research described in the work of Xu et al. [43] was to investigate the effect of AP binders, sintering additives (CuO and TiO_2), and calcination temperatures on dimensional stability, porosity, microstructure, and mechanical properties. The use of the addition of CuO and TiO_2 allowed the sintering of Al_2O_3 ceramics at lower temperatures. The authors developed the optimal composition and sintering conditions and obtained a ceramic material for 3D printing with high mechanical strength and low dimensional shrinkage and thus proved that aluminum dihydrogen phosphate can be used to print complex architectural features [43].

Titanium Oxide

Titanium oxide (TiO_2) is one of the materials that has been used in the printing of ceramics, both in pure form and in the form of an additive. TiO_2 is characterized by high photocatalytic activity and is also a material with antimicrobial properties [78]. Additionally, due to its high biocompatibility and osteoconductivity, titanium oxide can find potential application as a skeletal material for bone regeneration, as well as for various implants. Wang et al. [44] present in their work the preparation of bioceramic scaffolds (TiO_2) by means of direct-writing techniques. The direct technique allows better control over the appropriate pore structure of the scaffolding. TiO_2 sol-gel material for printing was prepared in a modified titanium diisopropoxide bisacetylacetonate (TIA) hydrolysis process. The selected printing methodology allows us to obtain 3D structures with a size of up to 10 µm with the possibility of obtaining controlled and regular pores [44].

In the literature, there are also examples of porous, hierarchical, and dense TiO_2 structures with specific mechanical properties [45]. The material for printing obtained by the authors of the work [45] consists of TiO_2, polyvinyl alcohol (PVA) as a binder, and zinc as a blowing agent. Foams with a porosity of up to 65% and an average pore size of 180 µm were obtained. The compacted samples had a modulus of elasticity of about 5 GPa and a compressive strength of about 100 MPa, while for the foam samples, the modulus of elasticity was 0.5 GPa, and the compressive strength was from 12 to 18 MPa. The tests show that the strength of the samples increases with the decrease in the porosity of the material. The next work also describes the preparation of hierarchical mesoporous TiO_2 cell architectures by 3D printing. The authors of the study combine two processes, i.e.,

direct foam writing with colloidal processing. The foam consists of TiO_2 nanoparticles, TALH (Ti(IV) bis (ammonium lactato) dihydroxide), which is an organic Ti precursor. After ink-foam preparation, the material was processed using continuous-flow direct writing and allowed to dry. After heat treatment, TALH is converted into TiO_2, promoting bridging between adjacent molecules, and resulting in the mechanical and chemical stability of the structures. The authors of the study obtained foams that are biocompatible, non-toxic, and stable in water; therefore, they are a potential application for biofunctionalization or as a biocomponent. The presented methodology in the work allows us to obtain variable properties in the surface morphology, pore size distributions, as well as various photocatalytic effects [46]. Xu et al. [47] in the publication describe the 3D printing method based on extrusion, which allows us to obtain hierarchical structures with macro and micro pores from metal oxide powders. Notably, 3D printed materials based on TiO_2, due to their structure and durability, can be used, among others, for filtration, thermal insulation, biomedical applications, and catalysts (including photocatalysts). The authors of the study compared TiO_2 structures obtained from nanoparticles (NP), submicron particles (MP), and mixed particles (NP/MP). The conducted rheological tests indicate non-Newtonian properties of materials prepared on the basis of TiO_2. One of the studies carried out by the authors of the study was the examination of the structural strength after heat treatment. The stress–strain curves were determined for the materials. Scaffolds made of NP/MP TiO_2 were characterized by maximum compressive strength at 600 °C (873 K) and 800 °C (1073 K), 0.082 MPa and 0.129 MPa respectively, while at 900 °C (1173 K) = 5.36 MPa. Volume shrinkage for NP samples was as much as 67.9% during heat treatment, while MP and N/MPa are characterized by slight changes during heat treatment and the volume shrinkage was 4.5% and 6.8%, respectively. Measurements of the specific surface area show that N/MP has the highest BET surface compared to NP and MP materials. X-ray powder diffraction measurements show that the heat treatment converts the crystalline phase of the NP sample from the anatase phase to the rutile phase with better crystallinity [47].

During the ceramic extrusion process, the material should have adequate wetting in order to facilitate processing. Binders are often used for this purpose. Optimization of materials can affect the production costs, as well as easier control of the process, and therefore the authors of [79] investigated the mechanical properties of a mixture of TiO_2 and an aqueous acid solution of the binder. The authors carried out viscosity determination studies using a capillary rheometer and a "cross-apparatus: rheometer:" developed at LMT Cachan. The processes involved mixing powder, acid, and water to form a paste, and then extruding it. The conducted research shows that the paste does not stick to the wall of the apparatus and does not slip according to the law of viscous friction and that the paste behaves completely differently from a viscous non-Newtonian fluid, which is probably due to the dissociation process taking place in the material. The conducted research allows for extending the characteristics of materials for printing ceramics.

Zirconium Oxide

Zirconium oxide is polymorphic and occurs in three allotropic forms: monoclinic, cubic and tetragonal. Each of the allotropes is stable in a different temperature range, e.g., the tetragonal phase is stable at a temperature of 1170 °C (1443 K) to 2360 °C (2633 K). However, this stability can be modified by adding other metal oxides such as yttrium oxide [80]. Zirconium ceramics (crystalline zirconium oxides) are characterized by high chemical stability, high mechanical strength, and good biocompatibility. This material has biomedical applications. It is used in dental restorations, hip joints, body implants, and bone fixings [48,81]. However, zirconia ceramics based on yttria-stabilized tetragonal polycrystalline zirconium oxide (Y-TZP) are currently used in biomedical applications. Y-TPZ is increasingly popular in dental applications, as it has high mechanical properties, biocompatibility, good fracture toughness, low thermal conductivity, good corrosion resistance, and good aesthetic properties [80,82].

The use of zirconium ceramics in 3D printing from pastes has been described in a limited amount of research. The authors investigate the properties of materials depending on the volume fraction of zirconium ceramics. In Peng et al. [49]'s work, the properties of materials printed from an aqueous ceramic suspension, which consisted of a commercial yttrium oxide stabilized zirconium powder (YZS) (solids content (<38 vol.%)), were investigated. Aqueous ceramic pasts were prepared by homogenizing YSZ powder with an appropriate amount of organic additives such as polyvinyl alcohol (PVA), polyethylene glycol (PEG-400), L-ascorbic acid (AA), and citric acid (CA). The element printed from the described paste and then sintered was characterized by a high density (>94%). Moreover, it retained the original morphology without any cracks or deformations with high linear shrinkage (approx. 33%).

Mohammadi et al. [50] evaluated the use of spray-dried commercial zirconia granules of 3 mol%. Stabilized with yttrium oxide, after intensive grinding, for the production of ceramic pastes. The starting material was spray-dried zirconium powder partially stabilized with 3 mol% yttrium oxide (in the form of granules or particles), to which was added Methocel (viscosity increasing agent, its purpose is to maintain homogeneity and prevent segregation of ceramic particles during printing), Darvan 821A (dispersant), glycerol (drying conditioner), Agitan299 (defoamer) and polyethyleneimine (gelling agent). The sample printed from the paste made of particles was characterized by a higher density before sintering; however, after sintering, the sample from the paste with granules had a higher density. Both sintered materials were characterized by a well-densified and fine microstructure. In addition, the samples printed from the paste with granules had fewer defects related to the decomposition of organic compounds. This can be explained by the fact that in these materials, there are large intermolecular spaces from which organic compounds were more easily removed.

3.2.2. Mixed Oxides

Lead Zirconate Titanate

Lead zirconate titanate (PZT) belongs to the group of so-called smart materials due to its piezoelectric properties and its use as a transducer in novel applications such as acoustic sensors, structural health monitoring, and energy harvesting [51]. Additive manufacturing combined with smart materials is called 4D printing, and therefore the PZT composite printing can be called 4D printing of ceramics [52].

Samuel E. Hall et al. [51] present in their work research on pastes PZT with varied water weight content to find a composition suitable for FDC printing. Particle size measurement using a scanning electron microscope (SEM), the PZT powder (Navy Type VI PZT ceramic powder) supplied by APC International (Mackeyville, PA, USA) consisted of spherical agglomerates with a diameter of 50–150 μm, and the individual PZT grains had an average diameter of 0.5 μm. For electrosteric stabilization, the ceramic particles received a coating with 1% polyelectrolyte—polyvinyl alcohol (PVA). The samples were evaluated for rheological properties and stability when aged. Pastes composed of less than 11 wt.% deionized water due to too high viscosity caused clogging of the nozzle and difficulties during the printing process. In turn, the addition of water over 14 wt.% caused the sagging of layers and material spreading after deposition. The observed large increase in viscosity was caused by the state of dispersion of PZT particles in the liquid. Increasing the content of ceramics resulted in a sudden aggregation and the formation of a gelled state unsuitable for extrusion. This phenomenon is caused by the forces of attraction between the particles, overcoming the dispersion by the medium and the surface of the PVA polyelectrolytes. The material properties of ceramics produced by the paste extrusion method were compared with those of the ceramics produced by the conventional die-pressing method. The relative permittivity of the printed sample after sintering was found to be 13.4% lower, but the piezoelectric properties were determined to be exceptionally close (within 0.1%) to samples obtained from die pressing. Aging tests showed that pastes were stable over a 24 h period [51].

In the work of K. Liu et al. [52] the results of research on printing with the composite material PZT core component of underwater acoustic transducer (devices that can convert acoustic and electrical signals into each other) FDC method are presented. The acoustic performance of this kind of ceramic can increase depending on the structure. Scientists have developed PZT slurry with high solid content and explored the influence of dispersants on rheological properties. It was found that 1.75 wt.% of ammonium polyacrylate used as a dispersant in the slurry exhibited the best printing effect. Ceramic frameworks differing in intervals between extruded rod fibers were printed. Pure trigonal perovskite structure is formed at the sintering temperature of the green body 1250 ÷ 260 °C (1523 ÷ 1533 K) and the relative density reaches 97.8%. With decreasing the distance between the extruded rods, the longitudinal piezoelectric strain coefficient (d_{33}) and dielectric constant (εr) of the piezoelectric composite first increase and then decrease. The best electrical performance of d_{33} = 103 pC/N and εr = 274.34 has been observed for the printed structure with a filling density of 26%. Printed samples of piezoelectric composites with the best electrical performance used to prepare underwater acoustic transducers also have the highest voltage output. The maximum output voltage was 162 mV. Notably, 4D printing with piezoelectric materials allows for the rapid introduction of structural changes, which makes it possible to achieve better performances [52].

Barium Titanate

Barium titanate ($BaTiO_3$—BT), an inorganic chemical compound that belongs to the known ferroelectric, pyroelectric, and piezoelectric materials, was discovered in the early 1940s. BT has been the first polycrystalline ceramic material discovered with ferroelectric properties [83]. $BaTiO_3$ ceramic materials are widely used, e.g., in capacitors, multilayer capacitors, sensors, and energy storage devices [84]. However, due to the brittleness of $BaTiO_3$ ceramics, new solutions for ceramic printing are being investigated, known processes are being optimized and the impact of various substances on the final effect and properties of materials is being studied.

Kim et al. [53] present an optimized method for 3D printing $BaTiO_3$ ceramics using paste extrusion. The ceramic suspension consists of $BaTiO_3$, polyvinylidene fluoride (PVDF), and N,N-dimethylformamide (DMF) solutions, which are both a binder, plasticizer, and dispersant, which allows us to obtain a high density of the final ceramic mass. The resulting ceramics were subjected to characteristic piezoelectric and dielectric properties. The highest BT density of 3.93 g/cm^3 was obtained by sintering at 1400 °C (1673 K), which resulted in significant grain growth (based on SEM, XRD). This allowed for high-performance piezoelectric and dielectric properties (200 pC/N and 4730 at 103 Hz, respectively). Notably, 3D-printed ceramics typically have a lower density compared to traditionally printed materials, resulting in poorer piezoelectric properties. Therefore, scientists [54] determine the effect of bimodal particle distribution on the density and piezoelectric properties of 3D printed ceramics and materials obtained by standard compression, as a reference sample. The materials consisted of $BaTiO_3$ (two different particle sizes), polyvinyl alcohol as the binder, and polyacrylic acid as a lubricant for slurry fabrication. The analysis showed that the samples obtained by both the 3D method and the traditional compression technique retain similar properties in terms of shrinkage and piezoelectric properties. The highest packing density was obtained by using a 50–50% vol. fraction. Printed samples had a maximum packing density of 35.99%, while compressed samples had 53.62% of the theoretical $BaTiO_3$ value. Shrinkage and density from small monodisperse particles to bimodal mixtures decreased depending on the dominant powder size, where the apparent inflection point was at 50–50% vol. Additionally, it was found that sample shrinkage is lower for bimodal mixtures with large particles. Materials obtained by printing using 50–50% vol. can be characterized by a piezoelectricity coefficient of 350 pC/N, which gives a value higher by 40% than the monodispersed sample using 100 nm particles [54]. Another work of this team concerns the influence of $BaTiO_3$ particle size (100 nm, 300 nm, 500 nm) on the final properties of the material obtained by freeze-form extrusion 3D printing. The

conducted tests indicated a higher density and better piezoelectric and dielectric properties for samples containing finer $BaTiO_3$ particles. The sample (100 nm $BaTiO_3$) had a density of 5.13 ± 0.35 g/cm^3, which correspond to 85.24 ± 5.74% of the theoretical value, piezoelectric properties of 204.61 ± 16.87 pC/N, which corresponds to 107.12 ± 8.83% of the theoretical value, and dielectric constant of 2551.09 ± 270 at 1 KHz, which is 115.38 ± 13.84% of the theoretical value. Using SEM, the morphology of the samples and grain size were examined. In addition, XRD analysis was performed to determine the crystal structure in the samples after sintering [55]. Renteria et al. in the article [56] describe the optimization of 3D printing parameters of $BaTiO_3$ ceramic materials affecting the piezoelectric coefficient, relative density, and dielectric permittivity by using design experiments with a 2k-1 design. The studies looked at the effects of $BaTiO_3$ particle size, polyvinyl alcohol (PVA) binder concentration, printing speed, and nozzle diameter. The conducted experiments indicate that the size of $BaTiO_3$ particles and the amount of binder in the material significantly affect the properties of the final material. The use of appropriately adjusted parameters allows for obtaining ceramic materials characterized by a piezoelectric coefficient higher than 200 pC/N and a density of 90% of the theoretical value of pure barium titanate.

3.2.3. Non-Oxides

Zirconium Diboride

Zirconium diboride (ZrB_2) belongs to the ultra-high-temperature ceramics (UHTC) group due to its excellent mechanical and physical properties such as high melting temperature, low density or great toughness and is a great object of interest for the ceramics industry [85]. In Sesso's et al. work [57], the FDC printing method was used to print multi-scale porous ultra-high-temperature ceramics. Zirconium diboride powders were used, from which aqueous suspensions were prepared, consisting of common ceramic binder polyvinyl alcohol (PVA) and ceramic powder. The printing paste consisted of 0.06 wt. surfactant sodium 1-heptanesulfonate (C7) (powder by weight) and sunflower oil. The final pastes contained from 60 to 70% by volume of oil and from 30 to 40% by volume of an aqueous suspension of ZrB_2. The test prints were made of a 37.5% volume of an aqueous suspension (containing a 25% volume of ZrB_2, a 4% volume of PVA powder, and a 0.06% volume of C7) and a 62.5% volume of sunflower oil. The tested pastes could be printed through nozzles with a diameter of 250 to 410 µm. The printed structures were usually characterized by porosity in the range of 72.5–77%, depending on the printing architecture and sintering temperature. The sintering temperature has a significant effect on porosity. The high temperatures and rapid heating of the furnace cause the segregation of particles in the oil phase, creating larger hollow structures. In the described work, the bending strength was tested. The bending strength ranged from 0.97 to 10.4 MPa with a characteristic strength of 3.58 MPa. The authors emphasized that the results obtained in the work are better compared to the strength-to-density ratio of printed materials from other oxide ceramics.

Nevertheless, research is underway on additives to improve these properties. The most common ZrB_2 additive to be found in the literature is silicon carbide fibers (SiC). ZrB_2 improves the properties of SiC. For example, the SiC-ZrB_2 composite has a higher thermal shock resistance than SiC alone. In addition, it was tested that at 20–30% vol., the SiC in ZrB_2 provides optimal oxidation resistance, but this is dependent on particle size and secondary phase network connections [58,59]. The addition of short, chopped fibers has been investigated by Kemp et al. [60]. In their work, objects were printed for tests using the FDC technique with the use of slurries with a composition of 47.5 vol% ZrB_2 and 10 vol% of SiC chopped fibers. The addition of SiC had a positive effect on the slurry flow properties, and thus on the printing process. The printed samples were subjected to pyrolysis. The conducted tests showed an increase in surface porosity. However, cracks appeared in the structure of the samples during the hardening and pyrolysis process. It is predicted that they may be caused by the difference in thermal expansion between SiC and ZrB_2 [60].

Silicon Carbide

Silicon carbide (SiC) is a widely chosen ceramic material, owing to its popularity due to properties such as high strength with low density, high thermal expansion, and great thermal conductivity. Notably, 3D printing is an increasingly popular method of obtaining ceramic structures with the use of SiC. Zhang et al. [61] prepared SiC suspensions with the addition of carbon black and chopped carbon fibers. The binder for the entire slurry was sodium alginate. The tested samples were obtained by 3D printing combined with liquid silicon infiltration. Two pastes for printing with different solids content were tested: 32.38 vol.% and 34.68 vol.%. It was concluded that the shrinkage on drying was less than 4% for each material and the shrinkage after sintering was less than 2%. In addition, the sintered composites were characterized by high flexural strength: 238 MPa and 300 MPa for materials with a solid content of 32.38 vol.% and 34.68 vol.%, respectively. The chopped carbon fibers were arranged directionally in the scaffolds parallel to the y-direction [61]. Chen et al. [62] also obtained structures using 3D printing, but as slurries for printing, they used n-hexane mixed with polycarbosilane (PCS). The printed shapes were pyrolyzed to obtain ceramic SiC structures. This work shows that obtaining ceramic SiC structures using a pre-ceramic material is an easy and effective method of 3D printing. The paper shows that the printed structure of the material with the addition of PCS can be processed by oxidative cross-linking and pyrolysis and transformed into SiC ceramics. It was noted that strong shrinkage occurred during pyrolysis; however, the printed SiC ceramic retained its structure.

Another example using the SiC-based composite in the FDC printing method is presented in Held et al.'s work [63]. Aqueous C-SiC pastes with solid particles (carbon powder, α-SiC powder) and a plasticizer were prepared. The solids content consisted of 10% by the weight of carbon powder and 90% by the weight of α-SiC powder. The dispersing medium was distilled water, dispersing agent (Tamol NN 9401), and glycerol. The tested pastes were characterized by a low content of organic additives, which allowed omitting the pyrolysis stage. The printability was determined by analyzing the effects of printing, such as overhang printing and bridging. The average volume accuracy between the CAD models and the printed element was about 3.4%. No defects were observed in the microstructure of the samples. The flexural strength was 190 MPa, and the hardness was 15.7 GPa. Additionally, phase analysis showed no residual free carbon in the materials [63].

In the works from the last year, it can be seen that ceramic pastes are reinforced with fibers, e.g., carbon. SiC composite reinforced with chopped carbon fiber (Cf/SiC) is a material with very good high-temperature properties and can be used in the aerospace and military industries [64]. The work of Liu et al. [65] presents the use of 3D printing for the production of Cf/SiC composites with high strength and low shrinkage. In this work, polycarbosilane (PCS) was used as a precursor to the ceramic SiC polymer, staple carbon fibers, n-hexane (PCS solvent), and toluene (auxiliary solvent preventing oxidation of the organic solvent in the printing process). Materials with different Cf content were tested, and mass fractions of Cf to PCS were 0 wt.%, 5 wt.%, 10 wt.%, 30 wt.%, and 50 wt.%, respectively. Rheological studies have shown that all ceramic pastes have good shear-thinning properties in the 3D printing process. In addition, it was indicated that the composite with 30 wt. Cf had the best flexural strength (~7.09 MPa) and the lowest linear shrinkage (~0.48%).

3.2.4. Bioceramics

Bioceramics are characterized by biocompatibility, durability, and the temperature of the sintering window. The most popular application of printed bioceramics is for bone tissue engineering, e.g., scaffolds, which are most commonly made from bioactive glasses and calcium phosphates such as hydroxyapatite (HA) [37,38]. Pure hydroxyapatite is not printed by the FDC method due to its state of aggregation and hardness. The material must have sufficient softness to be moldable; therefore, hydroxyapatite is mixed with the softening compounds [66]. In the work Zhong et al. [67], the extrusion process of hydroxyapatite (HA) paste during the printing of ceramic scaffolds was analyzed. Three factors influencing

the extrusion pressure were investigated, one of them was the paste composition. The following materials were used to prepare the ceramic paste: hydroxyapatite powder with a particle size of 1–5 µm (60% v/v), polyvinyl butyral (PVB) (75% w/v), and polyethylene glycol (PEG) (25% w/v) dissolved in a solvent, namely, propan-2-ol. PVB acts as a binder with hydroxyapatite, and PEG improves the flexibility of the material and reduces the viscosity; therefore, it acts as a plasticizer. The excess solvent is evaporated to obtain a suitable ceramic paste. Zhong et al. noted that the amount of solvent should be increased so as to have a minimal effect on extrusion pressure.

As mentioned earlier, in bioceramics printing, hydroxyapatite with binding and softening additives is used. The aim of the study by Roopavath et al. [68] was to simplify the materials and the process of print design. The binder additive used in their work was the reagent grade Hydroxy propyl methyl cellulose (HPMC). The printing paste was prepared in a proportion of 4 g of HA powder (particle size ~25 µm) to 2 g of 1.5 wt.%. HPMC solution, then thoroughly mixed to obtain a homogeneous, viscous ceramic mass. The applied polymer additive does not react with hydroxyapatite and is an inert material. Its task is to combine ceramic particles during printing and ensure the appropriate viscosity. In the analyzed work, scaffolds with a size of 10 mm × 10 mm × 7 mm with various filling (50%, 75%, and 100%) were printed. The mechanical properties of the obtained samples showed that as the filling density increases, cracks appear in various layers and a very irregular pattern of stress as a function of strain can be observed. Compression modules obtained after mechanical compression tests indicate an increase in mechanical strength along with an increase in the filling density, and the maximum (compression modulus) ~275 MPa occurs in scaffolding with 100% filling density.

Another bioceramic with good osteoinductive and osteoconductive properties is calcium phosphate (CaP). Additionally, calcium phosphate is a material of scientific interest in medical use, as its composition is similar to normal bone [69]. CaP occurs in enamel and bone in the form of multi-directional rods or plates [70,86]. It was thought that CaP synthesized in the laboratory would not have the same or similar properties as natural CaP. In the work of Zhang et al. [67], it was confirmed that synthetic CaP porous ceramics exhibit osteogenesis reactions in the tissue environment. In Dee et al. [87]'s work, pastes were prepared with CaP microplates. The first step was to prepare calcium hydrogen phosphate (brushite) from calcium chloride ($CaCl_2$), which was mixed with potassium dihydrogen phosphate (KH_2PO_4) and disodium hydrogen phosphate (Na_2HPO_4) in water. The resulting precipitate was dried to obtain brushite powder. The 3D printing paste consisted of various sizes of brushite microplates, a Dolapix CE 64 anionic surfactant, which is a dispersant, and polyvinylpyrrolidone (PVP), which is a binder. The prepared material was printed on plaster. In this study, it was found that the concentration of CaP microplates optimal for printing was at the level of 21–24% vol. The examination of the single-path microstructure after calcination shows that in the resulting fiber, the core-shell microstructure has a graded orientation of the microplates.

3.2.5. Clays

Clay is one of the oldest materials that has a wide range of uses and is still used by people. Clay is a mixture of hydrated oxides: SiO_2 and Al_2O_3 in a ratio of 2.0/1.0 to (4.0–5.0)/1.0. The most popular aluminosilicate material is kaolinite clay with the molecular formula: $2SiO_2 \cdot Al_2O_3 \cdot 2H_2O$. Kaolinite is a popular material because it is the most abundant in the earth's crust. Kaolinite is used to make ceramics, pottery, cosmetics, and paper [71,88]. The production of monolithic ceramic components by 3D printing poses challenges related to low powder packing density and the use of low-flowing powders. A common problem with clay printing is clogging of the nozzles as the drying process takes place during printing. Therefore, the clay composition is constantly modified by additives [7].

In the work of Revelo et al. [71], kaolinite clay from Colombia was tested. Samples were made from clays obtained with different water-to-clay ratios in the range of 0.65–0.69. In this work, the rheological properties of the pastes, compression tests, and Weibull analysis were

investigated. In Revelo's et al. work, clay without additives was found to have satisfactory properties as a material for use in art or the manufacture of structural parts. The best surface quality and rheological properties were achieved in the material with a water-to-clay ratio of 0.60. The Weibull distribution showed a large variability in compressive strength values ranging from about 20 to 50 MPa and a Weibull modulus from 4.5 to 6.3.

As mentioned earlier, clay is enriched with additives. Ordonez et al. [72] used two additives: sodium silicate and sodium polyacrylate at concentrations ranging from 0.2 to 0.8 wt.%. These additives were added to a typical ceramic paste supplied by Suministros de Colombia S.A.S. It has been found that the addition of sodium polyacrylate has a more significant effect as a deflocculant than the addition of sodium silicate. In addition, it was found that the best dimensional stability was shown by the sample with the addition of sodium polyacrylate in the amount of 0.8% and 53% of the volume fraction of the ceramic powder and the sample with the addition of sodium silicate (0.8%) and 50% of the volume fraction of the ceramic powder.

The same author [73] indicates the possibility of using steel dust waste from the electric arc furnace (EAFD). Three different water-to-clay ratios (0.50, 0.55, and 0.60) and different percentages of steel dust waste (0 wt.%, 10 wt.%, 20 wt.%, and 30 wt.%) were tested. The printed samples were dried for 24 h and then sintered for an hour at 1100 °C (1373 K) in air. Tests of mechanical properties (compression test) were carried out. From the analysis of the results in Ordonez's work, it was found that the maximum amount of EAFD dust was 20%, with a higher concentration, the nozzle was clogged. In addition, it was shown that the addition of dust improves compressive strength.

Faksawat et al. [74] used hydroxyapatite as the additional material, which was added to the clay provided by Boonsin Ceramic Co., Ltd. (Phra Pradaeng, Thailand) The chemical composition of clay and hydroxyapatite is given in Table 2.

Table 2. Chemical composition of clay provided by Boonsin Ceramic Co., Ltd. [74].

Chemical Compound	SiO_2	Al_2O_3	CaO	K_2O	MgO	Na_2O	TiO_2	Fe_2O_3	P_2O_5	Rb_2O
Mass content [%]	68.45	26.68	0.94	1.33	1.32	0.76	0.08	0.34	0.07	0.03

Clay was mixed with hydroxyapatite in proportions from 95:5% to 75:25% by weight, then distilled water was added to a ratio of 1:2. The suspension was stirred for 5 h and dried at room temperature for 24 h. The results showed that the samples where the weight ratio of clay to hydroxyapatite was 80:20 wt.% showed better print quality. In addition, these samples were characterized by good mechanical properties and low shrinkage after sintering (maximum bending strength and volumetric shrinkage of 88.72 MPa and 40.41%, respectively).

3.2.6. Cementitious Materials

The basic features that the cement material should have are ease of extrusion, flowability, good buildability, appropriate setting time and mechanical strength, the ability to obtain a continuous stream from the printing nozzle, and quick modeling of structures of any shape [89]. Increasing the stiffness of the liquid mixture in a short time after deposition from the nozzle is particularly important in large-scale 3DCP [90].

The consistency and physical properties of the cement should allow continuous transport through the tubing system and printhead nozzle. There are two methods most commonly used to improve the flow of cement mixes. The basic parameter determining the fluidity of cement pastes is the ratio of water to the binding material. However, too much water in the cement mix can lead to the deterioration of the material properties by increasing the number of pores or voids and reducing the mechanical strength [89].

In works on 3D printing with cement materials, the most common cement used in research is the so-called Ordinary Portland Cement, an exemplary composition of which is shown in Table 3 [75].

Table 3. The composition of Ordinary Portland Cement [88].

Chemical Compound	SiO_2	Al_2O_3	CaO	SO_3	Fe_2O_3	K_2O	TiO_2	LOI
Mass content [%]	18.7	4.4	68.1	5.24	2.7	0.56	0.32	0.98

Commonly used supplementary cementitious materials (SCM) are fly ash, blast furnace slag, and silica fume. These additives used in cement mixtures improve packing density, cohesion, and flow consistency. The addition of SCM can significantly affect the rheological properties of mixtures [90]. Zhenhua Duan et al. [75] published research on the effect of partial replacement of cement with metakaolin (MK) on a significant improvement in strength properties. Increasing the thixotropic surface area and reducing drying shrinkage results in improved buildability. MK has a positive effect on both fresh and cured material properties and is therefore recommended for use in 3DCP. As an example of printing with cement-based materials, we can distinguish 3D printing from concrete. Ali Kazemian et al. [76] published the test results of four different concrete mixes based on Type II Portland cement. The total content of cementitious materials and the ratio of water to cementitious materials in all blends were kept constant at 600 kg/m^3 and 0.43, respectively. It was found that acceptable print quality does not guarantee high dimensional stability because the four printing blends with acceptable print quality exhibited different levels of dimensional stability. Experimental data revealed that the addition of densified silica fume and highly purified attapulgite clay increased the shape stability of the fresh printing mixture, while relatively little improvement was observed with the addition of polypropylene fibers. The work entitled "Fiber-reinforced lightweight engineered cementitious composites for 3D concrete printing" by Junbo Sun et al. [77] describes the influence of polyvinyl alcohol fiber (PVA) and hollow glass microspheres (HGMs) on mechanical properties and the printability of concrete composites. It has been described that PVA fibers significantly reduced the slump loss and shortened the setting time, the opposite effect is shown by HGMs. The strength properties of the composites containing PVA fiber improved, while the opposite relationship was observed for the composites with the addition of HGMs. A significant anisotropy of the strength properties caused by the arrangement of the fibers in the composite was observed. The printing process affects the orientation of the fibers in the composite. Printed samples showed significantly higher strength values when tested with the fibers oriented in a direction perpendicular to the load.

3.2.7. Ceramic-Based Composite

A large increase in research on ceramic-based composite materials can be seen in the literature. Ceramics in composites can be used as a matrix or as reinforcement. In ceramic composites, in which ceramics are the matrix, reinforcements in the form of fibers, carbon nanotubes, graphene, or solid particles are often used. Such composites are characterized by good mechanical properties and stability at high temperatures [91].

Among the literature on 3D printing of ceramic composites using the FDC method, one can see a large application in biomedical engineering in the construction of scaffolds. An example of this is the work by Shao et al. [92], in which bioceramics with 10% Mg-doped wollastonite (CSi-Mg10) with 15% tricalcium phosphate (TCP15) were used for 3D printing. The scaffolds were characterized by good mechanical properties. The mechanical strength was above 80MPa and was 10 times higher than the scaffold obtained from the TCP material.

In addition, 3D printing is useful for the production of fillers and ceramics with excessive light scattering. In the work of Liu and Ding [93], 3D printing was used to produce CNT/Al_2O_3 composites. After printing, the models were sintered in argon. The electrical conductivity tests showed that composites containing 7 wt.% CNT were higher compared to monolithic alumina.

Recently, many scientists are working on the subject of 3D printing of ultra-high-temperature ceramic composites. An example of such a material is the ZrC/W composite.

In the work of Zahang et al. [94], 3D printing was combined with reactive infiltration. The first stage was to print the model from WC powders in a suspension consisting of dichloromethane, polystyrene, dibutyl phthalate, and ethylene glycol butyl ether. The printed models were then subjected to reactive melt infiltration by immersing these preforms in a bath of liquid $Zr_{14}Cu_{51}$. In another work [95], 3D printing was used to produce W/ZrC composites with a relative density of 70.1% and a flexural strength of only 31 MPa.

4. Comparison of Conventional Production and 3D Printing

Ceramics for technical applications are most often produced using the following methods: slip casting, including extrusion, injection molding, tape casting, as well as pressing and sintering. Pressing and sintering techniques are most often used to produce elements from ceramic powders. One of the popular methods is hot isostatic pressing (HIP), in which the material is obtained with high density and reduced or negligible porosity. The disadvantage of this method is the limited shapes of the manufactured elements. The manufactured elements are subjected to additional finishing machining, which increases the time and costs of production [96–98]. Another conventional method uses colloidal techniques that allow the production of ceramic parts close to the final shape, not requiring finishing processes [99]. The disadvantage of this method is the need to prepare appropriate molds and difficulties in casting. In addition, microcracks appear during the drying of ceramic elements, which affect the mechanical properties of the material [96]. In addition, gel casting, direct foaming, sacrificial template, frozen casting, and replica are used to produce porous ceramics [100]. However, most of these processes have complicated procedures, which significantly affect the cost and production time.

Notably, 3D printing of ceramics creates new possibilities for the production of elements with complex structures. An important advantage of using this technique is the ability to produce non-standard, low-volume parts, which reduces the cost of using tools for conventional manufacturing methods. In recent years, there has been a noticeable development in the 3D printing of polymeric and metallic materials. It is worth noting that many companies use this technology to supplement or replace conventional production methods. Due to the properties and processing of ceramics, the use of this material in 3D printing technology is more complicated [96,101].

The analysis of the literature shows that 3D printing of ceramics can primarily be used in the case of the need for components with complex shapes and porous. Obtaining high-density printed ceramics is a major challenge. The application of 3D printing to high-density materials is difficult due to the nature of the input material, such as the size and particle size distribution of ceramic powders, the number of organic additives, or the method of removing the binder. As a result, internal defects, high surface roughness, and the need for additional post-processing may appear in the printed elements [96,102].

5. Conclusions

Notably, 3D printing has recently aroused interest in many industries and has begun to fascinate many scientists. This technology is currently developing in two aspects: as a technology and the possibility of its modification, and in terms of materials from which components can be made. It is worth noting that the positive aspects resulting from the possibility of creating complex structures and cheap technology have influenced the development of materials used for 3D printing. In this work, an attempt was made to present groups of ceramic materials that are used in the 3D printing technology of ceramics from pastes. Ceramic pastes should be characterized by appropriate rheology; therefore, many works describe modifiers affecting the fluidity of pastes. One such additive is polyvinyl alcohol PVA, which improves the fluidity of pastes in which ceramics are added in the form of powders. The possibilities of using modifiers that are used for ceramic pastes were presented. The described technology is relatively new, so it should be further developed in the context of developing constant amounts of modifiers depending on the basic ceramics.

Author Contributions: Conceptualization, R.E.P., E.R.-R. and B.S.; methodology, R.E.P.; validation, E.R.-R., R.E.P. and B.S.; formal analysis, E.R.-R., R.E.P., B.S., D.P., E.G. and K.N.; data curation, E.R.-R.; writing—original draft preparation, R.E.P., E.R.-R., B.S., E.G., D.P. and K.N.; writing—review and editing, R.E.P.; visualization, E.R.-R. and D.P.; supervision, R.E.P.; project administration, E.R.-R. All authors have read and agreed to the published version of the manuscript.

Funding: This research received no external funding.

Data Availability Statement: The data used for the study was provided from the Scopus database analysis.

Acknowledgments: The authors would like to thank SYGNIS S.A. (SYGNIS New Technologies) for the support provided in the research carried out as part of the publication. Special thanks to CEO Andrzej Burgs.

Conflicts of Interest: The authors declare no conflict of interest.

References

1. Chaudhary, R.; Parameswaran, C.; Idrees, M.; Rasaki, A.; Liu, C.; Chen, Z.; Colombo, P. Additive Manufacturing of Polymer-Derived Ceramics: Materials, Technologies, Properties and Potential Applications. *Prog. Mater. Sci.* **2022**, *128*, 100969.
2. Huang, S.; Ye, C.; Zhao, H.; Fan, Z. Additive manufacturing of thin alumina ceramic cores using binder-jetting. *Addit. Manuf.* **2019**, *29*, 100802. [CrossRef]
3. Jinsong, C.; Enquan, B.; Dazhi, H.; Yunfei, D.; Xuhui, Q. Extrusion Freeforming-Based 3D Printing of Ceramic Materials. *Mater. Trans.* **2020**, *6*, 2236–2240. [CrossRef]
4. Chen, Z.; Li, Z.; Li, J.; Liu, C.; Lao, C.; Fu, Y.; Liu, C.; Yang, L.; Wang, P.; Yi, H. 3D printing of ceramics: A review. *J. Eur. Ceram. Soc.* **2019**, *39*, 661–687.
5. Bourell, D.; Kruth, J.; Leu, M.; Levy, G.; Rosen, D.; Beese, A.; Clare, A. Materials for additive manufacturing. *CIRP Annals* **2017**, *66*, 659–681.
6. Vaezi, M.; Chianrabutra, S.; Mellor, B.; Yang, S. Multiple Material Additive Manufacturing—Part 1: A Review. *Virtual Phys. Prototyp.* **2013**, *8*, 19–50. [CrossRef]
7. Zocca, A.; Colombo, P.; Gomes, C.; Günster, J. Additive Manufacturing of Ceramics: Issues, Potentialities, and Opportunities. *J. Am. Ceram. Soc.* **2015**, *98*, 1983–2001. [CrossRef]
8. He, R.; Zhou, N.; Zhang, K.; Zhang, X.; Zhang, L.; Wang, W.; Fang, D. Progress and challenges towards additive manufacturing of SiC ceramic. *J. Adv. Ceram.* **2021**, *10*, 637–674.
9. Vafadar, A.; Guzzomi, F.; Rassau, A.; Hayward, K. Advances in Metal Additive Manufacturing: A Review of Common Processes, Industrial Applications, and Current Challenges. *Appl. Sci.* **2021**, *11*, 1213. [CrossRef]
10. Martin, V.; Witz, J.; Gillon, F.; Najjar, D.; Quaegebeur, P.; Benabou, A.; Hecquet, M.; Berté, E.; Lesaffre, F.; Meersdam, M.; et al. Low cost 3D printing of metals using filled polymer pellets. *HardwareX* **2022**, *11*, e00292. [CrossRef]
11. Xiao, J.; Zhang, D.; Zheng, M.; Bai, Y.; Sun, Y.; Guo, Q.; Yang, J. 3D Printing of Metallic Structures using Dopamine-integrated Photopolymer. *J. Mater. Res. Technol.* **2022**, *19*, 1355–1366. [CrossRef]
12. Zhang, K.; Xie, C.; Wang, G.; He, R.; Wang, M.; Dai, D.; Fang, D. High solid loading, low viscosity photosensitive Al_2O_3 slurry for stereolithography based additive manufacturing. *Ceram. Int.* **2019**, *45*, 203–208. [CrossRef]
13. Xing, H.; Zou, B.; Li, S.; Fu, X. Study on surface quality, precision and mechanical properties of 3D printed ZrO_2 ceramic components by laser scanning stereolithography. *Ceram. Int.* **2017**, *43*, 16340–16347. [CrossRef]
14. Chang, C.; Lin, C.; Chang, C.; Liu, F.; Huang, Y.; Liao, Y. Enhanced biomedical applicability of ZrO_2–SiO_2 ceramic composites in 3D printed bone scaffolds. *Sci. Rep.* **2022**, *12*, 6845. [CrossRef]
15. Li, W.; Leu, M. Material Extrusion Based Ceramic Additive Manufacturing. In *Additive Manufacturing Processes*; ASM International: Novelty, OH, USA, 2020.
16. Gonzalez-Gutierrez, J.; Cano, S.; Schuschnigg, S.; Kukla, C.; Sapkota, J.; Holzer, C. Additive Manufacturing of Metallic and Ceramic Components by the Material Extrusion of Highly-Filled Polymers: A Review and Future Perspectives. *Materials* **2018**, *11*, 840. [CrossRef]
17. Hu, F.; Mikolajczyk, T.; Pimenov, D.; Gupta, M. Extrusion-Based 3D Printing of Ceramic Pastes: Mathematical Modeling and In Situ Shaping Retention Approach. *Materials* **2021**, *14*, 1137. [CrossRef]
18. Hu, F.; Cheng, J.; He, Y. Interactive design for additive manufacturing: A creative case of synchronous belt drive. *Int. J. Interact.Des. Manuf.* **2018**, *12*, 889–901.
19. Bourell, D.; Beaman, J.; Wohlers, T. History of Additive Manufacturing. In *Additive Manufacturing Processes*; ASM International: Novelty, OH, USA, 2020.
20. Wang, X.; Jiang, M.; Zhou, Z.; Gou, J.; Hui, D. 3D printing of polymer matrix composites: A review and prospective. *Compos. Part B Eng.* **2017**, *110*, 442–458.
21. Wohlers, T.; Campbell, I.; Diegel, O.; Huff, R.; Kowen, J. *Wohlers Report 2021: 3D Printing and Additive Manufacturing Global State of Theindustry*; Wohlers Associates: Fort Collins, CO, USA, 2021.

22. Additive Manufacturing Market Valued. Available online: https://additive-manufacturing-report.com/additive-manufacturing-market-2021/ (accessed on 15 January 2023).
23. *ISO/ASTM 52900*; Additive Manufacturing, General Principles, Terminology. International Organization for Standardization: Geneva, Switzerland, 2015.
24. Zafar, M.; Zhu, D.; Zhang, Z. 3D Printing of Bioceramics for Bone Tissue Engineering. *Materials* **2019**, *12*, 3361. [CrossRef]
25. Deckers, J.; Vleugels, J.; Kruth, J. Additive Manufacturing of Ceramics: A Review. *Ceram. Sci. Technol.* **2014**, *5*, 245–260.
26. Gmeiner, R.; Deisinger, U.; Schönherr, J.; Lechner, B.; Detsch, R.; Boccaccini, A.; Stampfl, J. Additive Manufacturing of Bioactive Glasses and Silicate Bioceramics. *J. Ceram. Sci. Tech.* **2015**, *6*, 75–86.
27. Ruscitti, A.; Tapia, C.; Rendtorff, N. A review on additive manufacturing of ceramic materials based on extrusion processes of clay pastes. *Ceramica* **2020**, *66*, 354–366. [CrossRef]
28. Muthukrishnan, S.; Ramakrishnan, S.; Sanjayan, J. Technologies for improving buildability in 3D concrete printing. *Cem. Concr. Compos.* **2021**, *122*, 104144. [CrossRef]
29. Sun, J.; Zhou, W.; Yan, L.; Huang, D.; Lin, L. Extrusion-based food printing for digitalized food design and nutrition control. *J. Food Eng.* **2018**, *220*, 1–11. [CrossRef]
30. Hussain, S.; Malakar, S.; Arora, V. Extrusion-Based 3D Food Printing: Technological Approaches, Material Characteristics, Printing Stability, and Post-processing. *Food Eng. Rev.* **2022**, *14*, 100–119. [CrossRef]
31. Li, W.; Ghazanfari, A.; Leu, M.; Landers, R. Extrusion-on-demand methods for high solids loading ceramic paste in freeform extrusion fabrication. *Virtual Phys. Prototyp.* **2017**, *12*, 193–205. [CrossRef]
32. Hinton, T.; Jallerat, Q.; Palchesko, R.; Park, J.; Grodzicki, M.; Shue, H.; Ramadan, M.; Hudson, A.; Feinberg, A. Three-dimensional printing of complex biological structures by freeform reversible embedding of suspended hydrogels. *Sci. Adv.* **2015**, *1*, e1500758. [CrossRef]
33. Huang, C. Extrusion-Based 3D Printing and Characterization of Edible Materials. Ph.D. Thesis, University of Waterloo, Waterloo, ON, Canada, 2018.
34. Wang, L.; Zhang, M.; Bhandari, B.; Yang, C. Investigation on fish surimi gel as promising food material for 3D printing. *J. Food Eng.* **2018**, *220*, 101–108. [CrossRef]
35. Carter, C.; Norton, M. *Ceramic Materials*; Springer: New York, NY, USA, 2013.
36. Lamnini, S.; Elsayed, H.; Lakhdar, Y.; Baino, F.; Smeacetto, F.; Bernardo, E. Robocasting of advanced ceramics: Ink optimization and protocol to predict the printing parameters—A review. *Heliyon* **2022**, *8*, e10651. [CrossRef]
37. Ben-Arfa, B.; Pullar, R. Comparison of Bioactive Glass Scaffolds Fabricated by Robocasting from Powders Made by Sol–Gel and Melt-Quenching Methods. *Processes* **2020**, *8*, 615. [CrossRef]
38. Del-Mazo-Barbara, L.; Ginebra, M. Rheological characterisation of ceramic inks for 3D direct ink writing: A review. *J. Eur. Ceram. Soc.* **2021**, *41*, 18–33. [CrossRef]
39. Ana, B.; Isabel, S.; Salvado, M.; Pullar, R.; Ferreira, J. Robocasting: Prediction of Ink Printability in Solgel Bioactive Glass. *J. Am. Ceram. Soc.* **2019**, *102*, 1608–1618.
40. Andrade, F.; Al-Qureshi, H.; Hotza, D. Measuring the plasticity of clays: A review. *Appl. Clay Sci.* **2011**, *51*, 1–7. [CrossRef]
41. Álvarez, F.; Cifuentes, A.; Serrano, I.; Franco, L.; Fargas, G.; Fenollosa, F.; Uceda, R.; Llanes, L.; Tardivat, C.; Llorca, J.; et al. Optimization of the sintering thermal treatment and the ceramic ink used in direct ink writing of α-Al_2O_3: Characterization and catalytic application. *J. Eur. Ceram. Soc.* **2022**, *42*, 2921–2930. [CrossRef]
42. Finke, B.; Hesselbach, J.; Schütt, A.; Tidau, M.; Hampel, B.; Schilling, M.; Kwade, A.; Schilde, C. Influence of formulation parameters on the freeform extrusion process of ceramic pastes and resulting product properties. *Addit. Manuf.* **2020**, *32*, 101005. [CrossRef]
43. Xu, X.; Zhang, J.; Jiang, P.; Liu, D.; Jia, X.; Wang, X.; Zhou, F. Direct ink writing of aluminum-phosphate-bonded Al_2O_3 ceramic with ultra-low dimensional shrinkage. *Ceram. Int.* **2022**, *48*, 864–871. [CrossRef]
44. Wang, R.; Zhu, P.; Yang, W.; Gao, S.; Li, B.; Li, Q. Direct-writing of 3D periodic TiO_2 bio-ceramic scaffolds with a sol-gel ink for in vitro cell growth. *Mater. Des.* **2018**, *144*, 304–309. [CrossRef]
45. Aleni, A.; Kretzschmar, N.; Jansson, A.; Ituarte, I.; St-Pierre, L. 3D printing of dense and porous TiO_2 structures. *Ceram. Int.* **2020**, *46*, 16725–16732. [CrossRef]
46. Arango, M.; Kwakye-Ackah, D.; Agarwal, S.; Gupta, R.; Sierros, K. Environmentally Friendly Engineering and Three-Dimensional Printing of TiO_2 Hierarchical Mesoporous Cellular Architectures. *ACS Sustain. Chem. Eng.* **2017**, *5*, 10421–10429. [CrossRef]
47. Xu, C.; Liu, T.; Guo, W.; Sun, Y.; Liang, C.; Cao, K.; Guan, T.; Liang, Z.; Jiang, L. D Printing of Powder-Based Inks into Functional Hierarchical Porous TiO_2 Materials. *Adv. Eng. Mater.* **2019**, *22*, 1901088. [CrossRef]
48. Jiaxiao, S.; Xie, B.; Zhu, Z. Extrusion-based 3D printing of fully dense zirconia ceramics for dental restorations. *J. Eur. Ceram. Soc.* **2022**, in press. [CrossRef]
49. Peng, E.; Wei, X.; Garbe, U.; Yu, D.; Edouard, B.; Liu, A.; Ding, J. Robocasting of dense yttria-stabilized zirconia structures. *J. Mater. Nauka.* **2018**, *53*, 247–273. [CrossRef]
50. Mohammadi, M.; Becker, G.; Diener, S.; Tulliani, J.; Katsikis, N.; Palmero, P. Robocasting of dense zirconia parts using commercial yttria-stabilized zirconia granules and ultrafine particles. Paste preparation, printing, mechanical properties. *Ceram. Int.* **2022**, *48*, 1936–1946. [CrossRef]

51. Hall, S.; Regis, J.; Renteria, A.; Chavez, L.; Delfin, L.; Vargas, S.; Haberman, M.; Espalin, D.; Wicker, R.; Lin, Y. Paste extrusion 3D printing and characterization of lead zirconate titanate. *Ceram. Int.* **2021**, *47*, 22042–22048. [CrossRef]
52. Liu, K.; Zhang, Q.; Zhou, C.; Shi, Y.; Sun, C.; Sun, H.; Yin, C.; Hu, J.; Zhou, S.; Zhang, Y.; et al. 4D Printing of Lead Zirconate Titanate Piezoelectric Composites Transducer Based on Direct Ink Writing. *Front. Mater.* **2021**, *8*, 659441. [CrossRef]
53. Kim, H.; Renteria-Marquez, A.; Islam, M.; Chavez, L.; Garcia Rosales, C.; Ahsan, M.; Tseng, T.; Love, N.; Lin, Y. Fabrication of bulk piezoelectric and dielectric $BaTiO_3$ ceramics using paste extrusion 3D printing technique. *J. Am. Ceram. Soc.* **2019**, *102*, 3685–3694. [CrossRef]
54. Renteria, A.; Garcia, L.; Balcorta, V.; Ortiz, D.; Delfin, L.; Regis, J.; Marcos-Hernandez, M.; Espalin, D.; Tseng, T.; Lin, Y. Influence of bimodal particle distribution on material properties of $BaTiO_3$ fabricated by paste extrusion 3D printing. *Ceram. Int.* **2021**, *47*, 18477–18486. [CrossRef]
55. Renteria, A.; Diaz, J.; He, B.; Renteria-Marquez, I.; Chavez, L.; Regis, J.; Liu, Y.; Espalin, D.; Tseng, T.; Lin, Y. Particle size influence on material properties of $BaTiO_3$ ceramics fabricated using freeze-form extrusion 3D printing. *Mater. Res. Express* **2019**, *6*, 115211. [CrossRef]
56. Renteria, A.; Fontes, H.; Diaz, J.; Regis, J.; Chavez, L.; Tseng, T.; Liu, Y.; Lin, Y. Optimization of 3D printing parameters for $BaTiO_3$ piezoelectric ceramics through design of experiments. *Mater. Res. Express* **2019**, *6*, 085706. [CrossRef]
57. Sesso, M.; Slater, S.; Thornton, J.; Franks, G. Direct ink writing of hierarchical porous ultra-high temperature ceramics (ZrB_2). *J. Am. Ceram. Soc.* **2021**, *104*, 4977–4990. [CrossRef]
58. Eakins, E.; Jayaseelan, D.; Lee, W. Toward oxidation-resistant ZrB_2-SiC ultra high temperature ceramics. *Metall. Mater. Trans.* **2011**, *42*, 878–887. [CrossRef]
59. Aguirre, T.; Lamm, B.; Cramer, C.; Mitchell, D. Zirconium-diboride silicon-carbide composites: A review. *Ceram. Int.* **2022**, *48*, 7344–7361.
60. Kemp, J.; Diaz, A.; Malek, E.; Croom, B.; Apostolov, Z.; Kalidindi, S.; Compton, B.; Rueschhoff, L. Direct ink writing of ZrB_2-SiC chopped fiber ceramic composites. *Addit. Manuf.* **2021**, *44*, 102049. [CrossRef]
61. Zhang, H.; Yang, Y.; Liu, B.; Huang, Z. The preparation of SiC-based ceramics by one novel strategy combined 3D printing technology and liquid silicon infiltration process. *Ceram. Int.* **2019**, *45*, 10800–10804. [CrossRef]
62. Chen, H.; Wang, X.; Xue, F.; Huang, Y.; Zhou, K. 3D printing of SiC ceramic: Direct ink writing with a solution of preceramic polymers. *J. Eur. Ceram. Soc.* **2018**, *38*, 5294–5300. [CrossRef]
63. Held, A.; Puchas, G.; Müller, F.; Krenkel, W. Direct ink writing of water-based C–SiC pastes for the manufacturing of SiC components. *Open Ceram.* **2021**, *5*, 100054. [CrossRef]
64. He, X.; Guo, Y.; Yu, Z.; Zhou, Y.; Jia, J. Study on microstructures and mechanical properties of short-carbon-fiber-reinforced SiC composites prepared by hot-pressing. *Mater. Sci. Eng. A* **2009**, *527*, 334–338. [CrossRef]
65. Liu, H.; Mei, D.; Yu, S.; Qian, S.; Wang, Y. Direct ink writing of chopped carbon fibers reinforced polymer-derived SiC composites with low shrinkage and high strength. *J. Eur. Ceram. Soc.* **2023**, *43*, 235–244. [CrossRef]
66. Ly, M.; Spinelli, S.; Hay, S.; Zhu, D. 3D Printing of Ceramic Biomaterials. *Eng. Regen.* **2022**, *3*, 41–52. [CrossRef]
67. Zhong, G.; Vaezi, M.; Liu, P.; Pan, L.; Yang, S. Characterization approach on the extrusion process of bioceramics for the 3D printing of bone tissue engineering scaffolds. *Ceram. Int.* **2017**, *43*, 13860–13868. [CrossRef]
68. Roopavath, U.; Malferrari, S.; van Haver, A.; Verstreken, F.; Rath, S.; Kalaskar, D. Optimization of extrusion based ceramic 3D printing process for complex bony designs. *Mater. Des.* **2019**, *162*, 263–270. [CrossRef]
69. Beniash, E.; Stifler, C.; Sun, C.; Jung, G.; Qin, Z.; Buehler, M.; Gilbert, P. The hidden structure of human enamel. *Nat. Commun.* **2019**, *10*, 4383. [CrossRef] [PubMed]
70. Zhang, B.; Pei, X.; Zhou, C.; Fan, Y.; Jiang, Q.; D'Amora, U.; Chen, Y.; Li, H.; Sun, Y.; Zhang, X. The biomimetic design and 3D printing of customized mechanical properties porous Ti6Al4V scaffold for load-bearing bone reconstruction. *Mater. Des.* **2018**, *152*, 30–39. [CrossRef]
71. Revelo, C.; Colorado, H. 3D printing of kaolinite clay ceramics using the Direct Ink Writing (DIW) technique. *Ceram. Int.* **2018**, *44*, 5673–5682. [CrossRef]
72. Ordoñez, E.; Gallego, J.; Colorado, H. 3D printing via the direct ink writing technique of ceramic pastes from typical formulations used in traditional ceramics industry. *Appl. Clay Sci.* **2019**, *182*, 105285. [CrossRef]
73. Ordoñez, E.; Monteiro, S.; Colorado, H. Valorization of a hazardous waste with 3D-printing: Combination of kaolin clay and electric arc furnace dust from the steel making industry. *Mater. Des.* **2022**, *217*, 110617. [CrossRef]
74. Faksawat, K.; Limsuwan, P.; Naemchanthara, K. 3D printing technique of specific bone shape based on raw clay using hydroxyapatite as an additive material. *Appl. Clay Sci.* **2021**, *214*, 10626. [CrossRef]
75. Duan, Z.; Li, L.; Yao, Q.; Zou, S.; Singh, A.; Yang, H. Effect of metakaolin on the fresh and hardened properties of 3D printed cementitious composite. *Constr. Build Mater.* **2022**, *350*, 128808. [CrossRef]
76. Kazemian, A.; Yuan, X.; Meier, R.; Khoshnevis, B. Performance-Based Testing of Portland Cement Concrete for Construction-Scale 3D Printing. *3D Concr. Print. Technol.* **2019**, *2019*, 13–35.
77. Sun, J.; Aslani, F.; Lu, J.; Wang, L.; Huang, Y.; Ma, G. Fibre-reinforced lightweight engineered cementitious composites for 3D concrete printing. *Ceram. Int.* **2021**, *47*, 27107–27121. [CrossRef]
78. Endo-Kimura, M.; Janczarek, M.; Bielan, Z.; Zhang, D.; Wang, K.; Markowska-Szczupak, A.; Kowalska, E. Photocatalytic and Antimicrobial Properties of Ag_2O/TiO_2 Heterojunction. *ChemEngineering* **2019**, *3*, 3. [CrossRef]

79. Chevalier, L.; Hammond, E.; Poitou, A. Extrusion of TiO_2 ceramic powder paste. *J. Mater. Process. Technol.* **1997**, *72*, 243–248. [CrossRef]
80. Kim, M.; Hong, M.; Min, B.; Kim, Y.; Shin, H.; Kwon, T. Microstructure, Flexural Strength, and Fracture Toughness Comparison between CAD/CAM Milled and 3D-Printed Zirconia Ceramics. *Appl. Sci.* **2022**, *12*, 9088. [CrossRef]
81. Khanlar, L.; Salazar Rios, A.; Tahmaseb, A.; Zandinejad, A. Additive Manufacturing of Zirconia Ceramic and Its Application in Clinical Dentistry: A Review. *Dent. J.* **2021**, *9*, 104. [CrossRef]
82. Zadeh, P.; Lumkemann, N.; Sener, B.; Eichberger, M.; Stawarczyk, B. Flexural strength, fracture toughness, and translucency of cubic/tetragonal zirconia materials. *J. Prosthet. Dent.* **2018**, *120*, 948–954. [CrossRef]
83. Acosta, M.; Novak, N.; Rojas, V.; Patel, S.; Vaish, R.; Koruza, J.; Rossetti, G.; Rödel, J. $BaTiO_3$-based piezoelectrics: Fundamentals, current status, and perspectives. *Appl. Phys. Rev.* **2017**, *4*, 041305. [CrossRef]
84. Buscaglia, V.; Buscaglia, M.; Canu, G. $BaTiO_3$-Based Ceramics: Fundamentals, Properties and Applications. *Encycl. Mater. Tech. Ceram. Glasses* **2021**, *3*, 311–344.
85. Feilden, E.; Glymond, D.; Saiz, E.; Vandeperre, L. High temperature strength of an ultra high temperature ceramic produced by additive manufacturing. *Ceram. Int.* **2019**, *45*, 18210–18214. [CrossRef]
86. Esslinger, S.; Gadow, R. Additive manufacturing of bioceramic scaffolds by combi- nation of FDM and slip casting. *J. Eur. Ceram. Soc.* **2020**, *40*, 3707–3713. [CrossRef]
87. Dee, P.; Tan, S.; Le Ferrand, H. Fabrication of Microstructured Calcium Phosphate Ceramics Scaffolds by Material Extrusion-Based 3D Printing Approach. *Int. J. Bioprint.* **2022**, *8*, 551. [CrossRef]
88. Ríos, C.; Williams, C.; Fullen, M. Hydrothermal Synthesis of Hydrogarnet and Tobermorite at 175 °C from kaolinite and metakaolinite in the $CaO–Al_2O_3–SiO_2–H_2O$ system: A comparative study. *Appl. Clay Sci.* **2009**, *43*, 228–237. [CrossRef]
89. Ma, G.; Wang, L.; Ju, Y. State-of-the-art of 3D printing technology of cementitious material—An emerging technique for construction. *Sci. China Technol. Sci.* **2018**, *61*, 475–495. [CrossRef]
90. Chen, Y.; He, S.; Gan, Y.; Çopuroğlu, O.; Veer, F.; Schlangen, E. A review of printing strategies, sustainable cementitious materials and characterization methods in the context of extrusion-based 3D concrete printing. *J. Build. Eng.* **2022**, *45*, 103599. [CrossRef]
91. Sun, J.; Ye, D.; Zou, J.; Chen, X.; Wang, Y.; Yuan, J.; Liang, H.; Qu, H.; Binner, J.; Bai, J. A review on additive manufacturing of ceramic matrix composites. *J. Mater. Sci. Technol.* **2023**, *138*, 1–16. [CrossRef]
92. Shao, H.; Liu, A.; Ke, X.; Sun, M.; He, Y.; Yang, X.; Fu, J.; Zhang, L.; Yang, G.; Liu, Y.; et al. 3D robocasting magnesium-doped wollastonite/TCP bioceramic scaffolds with improved bone regeneration capacity in critical sized calvarial defects. *J. Mater. Chem. B* **2017**, *5*, 2941–2951. [CrossRef]
93. Liu, C.; Ding, J. Carbon nanotubes reinforced alumina matrix nanocomposites for conductive ceramics by additive manufacturing. *Procedia Manuf.* **2020**, *48*, 763–769. [CrossRef]
94. Zhang, D.; Kenel, C.; Caccia, M.; Sandhage, K.; Dunand, D. Complex-shaped, finely-featured ZrC/W composites via shape-preserving reactive melt infiltration of porous WC structures fabricated by 3D ink extrusion. *Addit. Manuf. Lett.* **2021**, *1*, 100018. [CrossRef]
95. Li, A.; Thornton, A.; Deuser, B.; Watts, J.; Leu, M.; Hilmas, G.; Landers, R. Freezeform extrusion fabrication of functionally graded material composites using zirconium carbide and tungsten. In Proceedings of the 23rd Annual International Solid Freeform Fabrication Symposium, Austin, TX, USA, 6–8 August 2012; pp. 467–479.
96. Olhero, S.; Torres, P.; Mesquita-Guimarães, J.; Baltazar, J.; Pinho-da-Cruz, J.; Gouveia, S. Conventional versus additive manufacturing in the structural performance of dense alumina-zirconia ceramics: 20 years of research, challenges and future perspectives. *J. Manuf. Process.* **2022**, *77*, 838–879. [CrossRef]
97. Abyzov, A. Aluminum Oxide and Alumina Ceramics (Review). Part 2. Foreign Manufacturers of Alumina Ceramics. Technologies and Research in the Field of Alumina Ceramics. *Refract. Ind. Ceram.* **2019**, *60*, 33–42. [CrossRef]
98. Klocke, F.; Iqbal, I.; Nath, R.; Bora, L.; Singh, B.; Mandal, N. Modern Approaches for the Production of Ceramic Components. *J. Eur. Ceram. Soc.* **1997**, *17*, 457–465. [CrossRef]
99. Franks, G.; Tallon, C.; Studart, A.; Sesso, M. Colloidal processing: Enabling complex shaped ceramics with unique multiscale structures. *J. Am. Ceram. Soc.* **2017**, *100*, 458–490. [CrossRef]
100. Zhang, F.; Li, Z.; Xu, M.; Wang, S.; Li, N.; Yang, J. A review of 3D printed porous ceramics. *J. Eur. Ceram. Soc.* **2022**, *42*, 3351–3373. [CrossRef]
101. Ngo, T.; Kashani, A.; Imbalzano, G.; Nguyen, K.; Hui, D. Additive manufacturing (3D printing): A review of materials, methods, applications and challenges. *Compos. Part B* **2018**, *143*, 172–196. [CrossRef]
102. Choppala, S.; Allam, A.; Fang, Z.; Armani, A. Next generation of advanced ceramic 3D printers. *Future Technol.* **2022**, *2*, 36–42. [CrossRef]